Analysis of the Influence of Color Normalization in the Classification of non-Hodgkin Lymphoma Images

Matheus G. Ribeiro *, Leandro A. Neves *, Guilherme F. Roberto †,
Thaína A. A. Tosta ‡, Alessandro S. Martins § and Marcelo Z. do Nascimento †
* Department of Computer Science and Statistics (DCCE),
São Paulo State University (UNESP), São José do Rio Preto, São Paulo, Brazil.
E-mail: goncalves.ribeiro@unesp.br
† Faculty of Computation (FACOM), Federal University of Uberlândia (UFU), Uberlândia, Minas Gerais, Brazil.
‡ Center of Mathematics, Computing and Cognition, Federal University of ABC, Santo André, São Paulo, Brazil
§ Federal Institute of Triângulo Mineiro (IFTM), Ituiutaba, Minas Gerais, Brazil.

***Abstract*—In this work, a method is proposed to analyze the influence of color normalization in the classification lymphoma images. The approach combines multidimensional fractal techniques, curvelet transforms and Haralick features. The method considered a feature selection technique and different classification approaches to evaluate the combinations, such as decision tree, random forest, support vector machine, naive bayes and k-star. The classifications were analyzed considering three common lymphoma classes: mantle cell lymphoma, follicular lymphoma and chronic lymphocytic leukemia. The best result was achieved for the extraction from input images, features obtained mostly from lacunarity and percolation from curvelet sub-images, using random forest classifier. The tests were considered with 10-fold cross-validation and the result was a rate of $AUC = 0.963$. The color normalization was not able to provide relevant classification rates. The obtained performance with the analysis over different types of features, classifiers and color normalization influence are important contributions to the identification of the lymphoma cancer.**

I. Introduction

Lymphoma is a cancer originated on the lymphatic system, which is classified into two types: Hodgkin (HL) and non-Hodgkin (NHL), categorized according to the pattern of growth and citological characteristics from the cells [1]. In the United States for the year of 2018, 8,500 new HL cases and 74,680 NHL new cases were estimated, causing an estimated of 1,050 deaths by HL and 19,910 by NHL [2]. In Brazil, an estimation was performed by the Institute National of Cancer (INCA) for the biennium 2018-2019, with 5,370 new cases for men and 4,810 for women considering NHL [3]. The main research focus related to this area of cancer concentrate in non-Hodgkin lymphomas due to the higher rate of incidence.

The NHLs are divided into a variety of sub-types: mantle cell lymphoma (MCL), follicular lymphoma (FL) and chronic lymphocytic leukemia (CLL). MCL sub-type affects frequently individuals over 50 years, which represents 4% of all lymphomas in the United States. FL lymphomas constitutes around 50% of adult lymphomas. CLL is the most common type of leukemia, affecting patients mostly over 60 years [4].

The most common method considered by pathologists for diagnosing NHL consists on tissue samples stained with hematoxylin-eosin (H&E). This task is challenging and time consuming for pathologists, mainly when the objective is to classify the correct type of NHL [1]. In order to minimize the related problems, computational methods were proposed to support pathologists in the pattern classification and recognition task of non-Hodgkin lymphomas stained with H&E [5]–[7]. The success of each method can be attributed partly by the feature extraction stage.

Different approaches can be applied to perform the feature extraction, such as the techniques presented in this work: Haralick features, fractal approaches and curvelet transform. For instance, Haralick features [8] are useful to extract statistical properties of the texture, with important applications in different contexts, such as detect epileptic activity [9], diagnose glaucoma [10] and study the oral cancer [11]. Also, autosimilarity properties are extracted mostly from fractal features. The main approaches are fractal dimension (FD), lacunarity (Lac) and more recently, percolation (Perc). FD quantifies the complexity and irregularity of a fractal, analyzing the level of space filling of the image [12]. The Lac indicates how the pixels are distributed and organized across an image. The Perc consists of the occurrence of a path that connects the upper to the lower part of a fractal [13]. The different fractal approaches were applied to study glaucoma [14], breast cancer [15], prostate cancer [16] and non-Hodgkin lymphomas [7]. The curvelet transform was also applied to classify the different degrees of prostate cancer [17], diagnose breast cancer [18] and study cerebrovascular and neoplastic diseases [19].

The feature extraction has an important role in systems developed for the identification of lymphomas. In addition, researches have been addressed to show that the preprocessing step can also provide an important role in this task [20], [21]. One of the approaches applied on the preprocessing step is color normalization [22]. This technique is relevant by reducing the color variation caused by differences in color

responses of slide scanners and environmental aspects such as lighting variation [21], [23]. This variation can produce difficulties for the specialist and also affect the efficiency of the methods developed to support the diagnosis. Therefore, in this work a method is proposed that associates multiscale and multidimensional fractal features, Haralick descriptors and curvelet sub-images to extract features from the lymphomas H&E stained images. Furthermore, the extraction was performed in non-normalized and color normalized images to compare the differentiation rates in order to analyze the influence of color normalization in the classification step. In this way the main contributions are:

- A combination of features that provides relevant distinction rates when classifying non-Hodkgin lymphomas;
- A comparison of the classification performance with the proposed extraction approaches from non-normalized and color normalized images.

II. Methodology

The proposed methodology was organized into 4 stages. In stage 1, feature extraction was performed by considering multiscale and multidimensional methods (FD, Lac and Perc features) and Haralick descriptors. The features were extracted from the non-normalized and color normalized images, as well as the corresponding curvelet sub-images. Stage 2 comprised the feature selection for the classification of the lymphomas. In stage 3, the classifiers decision tree (DT), support vector machines (SVM), random forests (RaF), naive bayes (NB) and K-star (K*) were applied to differentiate the studied groups. The last stage was the performance evaluation, considering the analysis of the best combinations and results. A general view of the method is presented in Fig 1.

A. Image color normalization

The process of staining and scanning tissue samples through microscopic examination may lead to undesirable variations in color, due to the response of digital scanners and the staining protocols. Thus, the process of normalization may aid the laboratory analysis and pattern recognition systems [21]. Different techniques of color normalization were proposed in the literature [21], [24], [25].

In this work, the normalization technique described by Vahadane et al. [21] was applied in order to compare the influence of the color normalization in the process of feature extraction in lymphoma images. The applied technique is called structure-preserving color normalization (SPCN), which performs the stain separation and color normalization, preserving the biological structure information by modeling stain density maps based on the properties of non-negativity, sparsity and soft-classification [21]. This approach basically works with the replacement of the color basis from the H&E image with those preferred from pathologists, while keeping the original stain concentrations. The SPCN approach also captures most of the histological structures in the stain concentration [21].

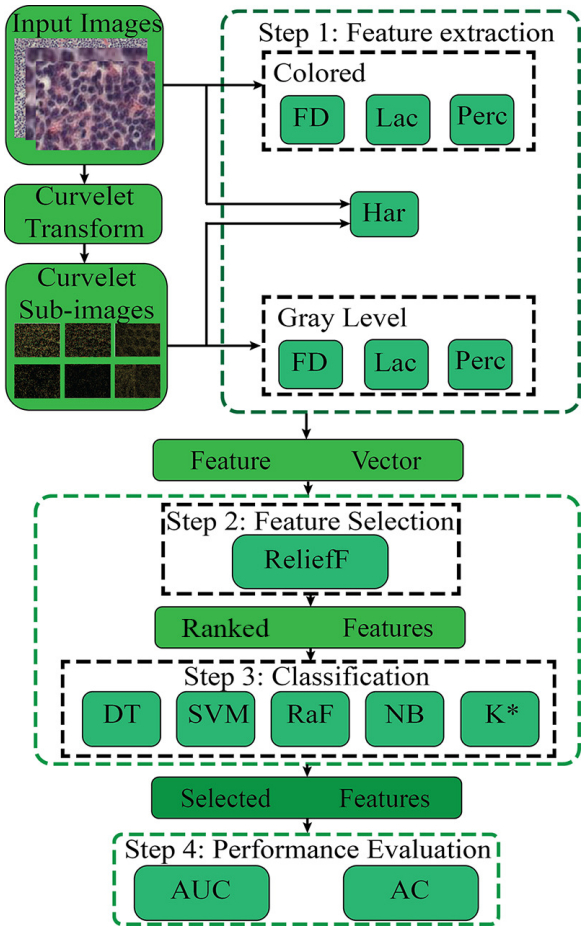

Fig. 1. A summary of the proposed methodology for evaluating lymphoma images considering non-normalized and color-normalized images.

B. The curvelet transform

The curvelet transform was applied to generate sub-images from the NHL (non-normalized images and color normalized images). In this study, the applied approach was the fast discrete curvelet transform with the wrapping function [26]. This approach is based on the Fourier samples considering the image as a Cartesian matrix $f[r, s]$, where $0 \leq r < R$, $0 \leq s < S$, R and S are the dimensions of the matrix. The obtained results were curvelet coefficient sets $c^D(j, l, \rho_1, \rho_2)$ with a scale j, direction l and spatial localization parameters ρ_1 and ρ_2 (Eq. 1).

$$c^D(j, l, \rho_1, \rho_2) = \sum_{n=1}^{R} \sum_{m=1}^{S} f[r, s] \varphi^D_{j,l,\rho_1,\rho_2}[r, s]. \quad (1)$$

The curvelet coefficient set consisted of parallelograms that contained a digital curvelet in the form of a wave $\varphi^D_{j,l,\rho_1,\rho_2}$. The wrapping consisted of collecting the information through the parallelograms inside the rectangle, centered at the origin, with a width of $2^{j/2}$ and height of 2^j.

The curves contained on each image were represented by gaps along the neighbor gray levels. The curvelets were numerical values that represent the curves in coefficients. The

parameters considered for curvelet calculation were 4 scales and 8 rotations, according to the information presented by [27], [28]. The results were 41 curvelet sub-images for each given histological H&E lymphoma image.

C. Fractal techniques

The fractal features were calculated after obtaining the curvelet sub-images. The fractal methods performed in this work were fractal dimension, lacunarity and percolation. In the Literature, there are fractal dimension approaches that are multiscale and multidimensional, which are capable of quantifying images in color or in gray scale level. In this context, the main FD approaches are the probabilistic method from Ivanovici, Richard and Decean [29] and the box merging approach from Nikolaidis N., Nikolaidis I. and Tsouros [30]. The probabilistic approach was also applied to calculate the lacunarity [29]. The percolation model was obtained from the approach proposed by Roberto et al. [7]. These techniques were applied to extract features from the colored lymphoma histological images and from the gray level sub-images. The sub-images were obtained by applying the curvelet transform.

1) Fractal dimension based on probabilistic approach: The probabilistic method [29] was applied by considering a box of side L scanning all pixels of the image (RGB color model) given as input. Thus, given a box of size L positioned over the image with the central pixel (F_c), the color channel with more relevance was selected by comparing F_c with the remaining pixels F from the box under analysis. The distance of the pixels $F = f(x, y, r, g, b)$ to the central pixel $F_c = f_c(x_c, y_c, r_c, g_c, b_c)$ were obtained by applying the Minkowski distance (Eq. 2), where the values of x and y indicate the location of the pixel on the image and the values of r, g and b correspond to the channel intensities. If the maximum value obtained was less or equal than L, the pixel is considered to belong to the box. The sum and storage on a probability matrix $P(m, L)$ is performed, which represents the probability of m points belonging to a box on its side L.

After applying the multiscale and multidimensional approaches, the total number of boxes $N_{FD_p}(L)$ for covering an image was defined (Eq. 3) and calculated for different observation scales L. The probabilistic fractal dimension FD_p was given by the angular coefficient of the linear regression defined by $\log L \times \log N_{FD_p}(L)$. The size of the boxes were $L = 3$ to $L = 45$. These values were sufficient for indicating multiscale observations in lymphoma images.

$$|F - F_c| = max|f(i) - f_c(i_c)| \leq L, \forall i = \overline{1, 5}, \quad (2)$$

$$N_{FD}(L) = \sum_{m=1}^{N} \frac{P(m, L)}{m}. \quad (3)$$

2) Fractal dimension based on box merging approach: The box merging FD_m [30] was another approach to obtain the fractal dimension. The calculation similarly to the other fractal approach was performed on input lymphoma images and generated curvelet sub-images. The value of FD_m was determined from a partition table defined as in Eq.4, where L is an observation scale, s indicates the size of the partition under analysis, x is the coordinate of a pixel in the box and ϵ indicates the relation of L/s. The table allows the storage of all the partition coordinates t that contains at least one element from the dataset. Each line indicates the calculation of the partitions t_x, t_y, t_r, t_b, t_g for each pixel of the image. The quantity of lines n_m on the partition table is counted at each iteration. The value of FD_m was obtained from the angular coefficient of a graph of $\log n_m \times \log s$.

$$t_x = \left\lfloor \frac{x}{\epsilon_x} \right\rfloor = \left\lfloor \frac{xs}{L_x} \right\rfloor. \quad (4)$$

3) Multiscale and multidimensional percolation: The percolation can be defined as the existence of a path of connected pixels (cluster) from one extremity to the other from an image. The applied method was described in detail by Roberto et al. [7].

The first step consisted of a multiscale analysis with the gliding box algorithm. A square box with a side of L was used to cover all the pixels of an image, increasing the size L after covering the image entirely. The box total T was calculated from width W and height H of the image as well the box size of L (Eq. 5).

$$T = (H - L + 1) \times (W - L + 1). \quad (5)$$

In the next step, the multidimensional analysis was performed by applying the Minkowski distance (Eq. 2), as defined for calculating the FD_p. When the Minkowski distance d was less or equal to L, the value of P was defined as -1 to indicate the representation of a pore in the considered box.

The third step was defined to associate the percolation theory with the multiscale and multidimensional approaches. Thus, the height and width of the matrix, as well as the probability p were applied to define a pore whereby a supposed fluid may flow through it. The remaining spaces correspond to solids where the fluid is not able to flow [7]. The presence of a percolating cluster is guaranteed when p is greater than the percolating threshold ($p = 0.59275$) [31]. The cluster labeling algorithm of Hoshen-Kopelman was applied to obtain the percolating clusters based on the values of $P = -1$ [32].

The analysis of lymphoma images was performed with three functions: cluster average C, percolating box ratio Q and average coverage ratio of the largest cluster Γ. The number of clusters in a box is given by c_i and the average per box $C(L)$ is presented in Eq. 6.

$$C(L) = \frac{\sum_{i=1}^{T} c_i}{T}. \quad (6)$$

The percolating boxes ratio Q consisted of the number of percolated boxes divided by the total number of box T in a scale L. A box q_i was considered as a percolating box if the ratio between the number of pixels labeled as pores (Ω_i) and the total number of pixels inside the box (L^2) exceeded the

percolation threshold p. Thus, the function $Q(L)$ was obtained by dividing the total number of percolating boxes q_i by the total number of boxes T in a specified scale L, as in Eq. 7.

$$Q(L) = \frac{\sum_{i=1}^{T} q_i}{T}. \quad (7)$$

The coverage ratio of the largest cluster in each box of size L was given by the function of the average coverage ratio of the largest cluster Γ. The coverage of a box i consisted in the division of its largest cluster (γ_i) by the number of pixels in the box L^2 (Eq. 8).

$$\Gamma(L) = \frac{\sum_{i=1}^{T} \gamma_i / L^2}{T}. \quad (8)$$

The behaviors of the functions $C(L)$, $Q(L)$ and $\Gamma(L)$ were analyzed by considering different metrics: area under curve (ARC), skewness (SKW), area ratio (AR), maximum point (MP) and the scale of the maximum point (SMP). These metrics were described by Roberto et al. [7]. The percolation approach was obtained by applying box sizes of $L = 3$ to $L = 45$. These values are similar to those used in the calculation of FD_p.

4) Lacunarity: The pixel distribution and organization were quantified by applying the methods described by [33], [34]. The lacunarity $Lac(L)$ was obtained from colored images and curvelet sub-images. The applied approach for multidimensional lacunarity was the method proposed in [29] by calculating the first order moment (Eq. 9) and second order moment (Eq. 10). These moments were defined based on the probability matrix $P(m, L)$.The calculation of $Lac(L)$ is presented in Eq. 11. The lacunarity curves were analyzed by applying the metrics ARC, SKW, AR, MP and SMP, considering the work presented by Roberto et al. [7].

$$\lambda(L) = \sum_{m=1}^{N} mP(m, L), \quad (9)$$

$$\lambda^2(L) = \sum_{m=1}^{N} m^2 P(m, L), \quad (10)$$

$$Lac(L) = \frac{\lambda^2(L) - (\lambda(L))^2}{(\lambda(L))^2}. \quad (11)$$

D. Haralick features

Haralick features were also applied to evaluate the H&E images and the curvelet sub-images. The features were calculated from the co-occurrence matrices [8]. In this study, the values considered were of distance $\delta = 1$ and orientation $\theta = 0°$, $\theta = 45°$, $\theta = 90°$ and $\theta = 135°$. The Haralick features were calculated from the average values of the obtained co-occurrence matrices: (1) angular second moment; (2) contrast; (3) correlation; (4) sum of squares (variance); (5) inverse difference moment; (6) sum average; (7) sum variance; (8) sum entropy; (9) entropy; (10) difference variance; (11) difference entropy; (12) and (13) are information measures of correlation; (14) maximal correlation coefficient. The features were applied as proposed by [8].

E. Composition of the feature vector

The features were defined by associating the previously described approaches: a value of FD_p; a value of FD_m; 5 values of Lac (ARC, SKW, AR, MP and SMP), represented by Lac(1) until Lac (5); 14 Haralick features, represented by Har(1) until Har(14); and, 15 percolation features (ARC, SKW, AR, MP and SMP) for each function (C, Q, Γ), named Perc(1) to Perc(15). These features were calculated for curvelet sub-images, with parameters of 4 scales and 8 rotations. The results were 41 sub-images for each lymphoma image. Thus, the feature vector was composed by 1512 values (Fig. 2).

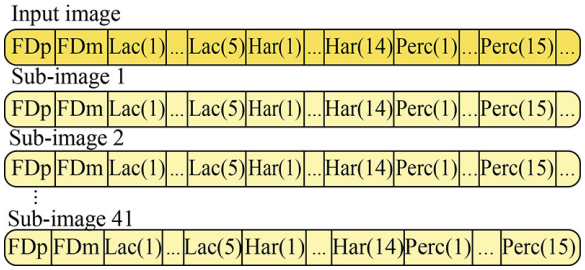

Fig. 2. Illustration of the feature vector obtained with fractal approaches and Haralick features, considering the non-normalized and normalized images, as well as the corresponding curvelet sub-images.

F. Classification and evaluation of features

The dimensionality of the feature vector with 1512 values was reduced by applying the ReliefF algorithm [35]. This algorithm is an expansion of Relief approach [36]. The goal was to define the most relevant features to understand the lymphoma cancer. Each reduced feature vector was evaluated by applying different classifiers, such as DT [37], SVM [38], RaF [39], NB [40] and K* [41]. The approach of $k-$fold cross-validation was applied to these algorithms with $k = 10$. The method was evaluated by considering two metrics: area under the ROC curve (AUC) and accuracy (AC) [42].

The feature selection was performed over each fold k to rank the most relevant features. The number of features was obtained by observing the average performance of the folds. This strategy was performed by considering the AUC metric. The approach started with 5 features, adding 5 at each iteration until reaching 100 features. The total number of features was defined by counting the number of features at each fold, without repetitions. This approach was achieved with the analysis of the size of the union of the folds.

In this work, the feature extraction approaches were implemented by using the MATLAB software, version R2015a, and the Weka platform 3.8.1 [43]. The curvelet coefficients were calculated by applying the curvelab package [44].

G. Image Database

The proposed work was tested on NHL images from the National Cancer Institute [45] and from the National Institute on Aging [46]. The image database consisted on 173 histological NHL images comprising by 99 images from MCL group,

62 from FL group and 12 representing the CLL group. The images were digitally acquired, through a light microscope (Zeiss Axioscope) with a 20 objective and a colored digital camera (AXio Cam MR5). The regions of interest were selected by specialists, digitally photographed and recorded without compression, with the RGB color model and spatial resolution of 1388×1040 pixels. In Figs. 3, 4 and 5 examples are presented for the MCL, FL and CLL groups, respectively.

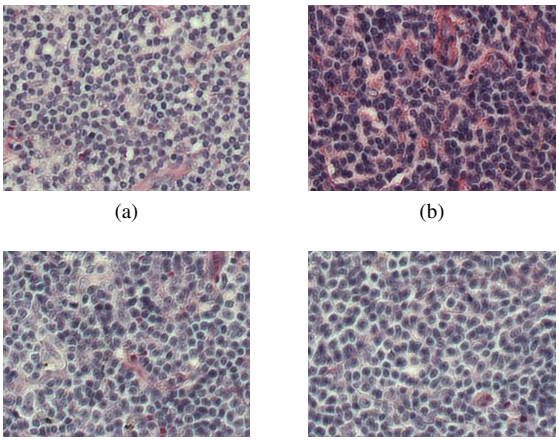

(a) (b) (c) (d)

Fig. 3. Examples of MCL histological images group.

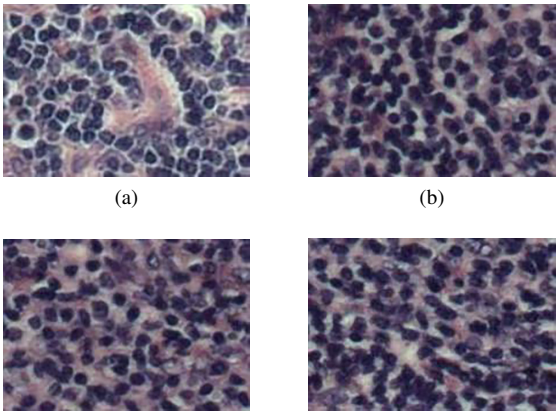

(a) (b) (c) (d)

Fig. 4. Examples of FL histological images group.

III. Results

The color normalization was performed in the image dataset (Figs. 3, 4 and 5), considering the approach presented in subsection II-A. The results were color normalized images. Examples of the images after this stage are presented in the Figs. 6, 7 and 8.

The curvelet transform was applied in the non-normalized H&E images as well as in the color normalized ones, considering scales of 1 to 4 and rotation of 1 to 8. The results were 41 curvelet sub-images. The approaches for obtaining FD_m, FD_p, Lac, Har and $Perc$ were used to quantify each input and normalized images as well as the corresponding curvelet sub-images. The feature selection step was applied at each fold to obtain the most relevant features among the 1512

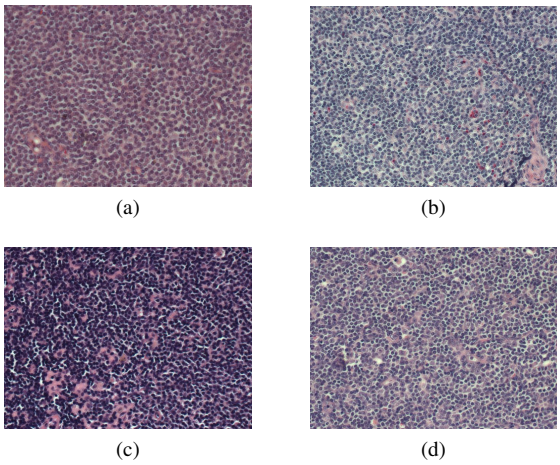

(a) (b) (c) (d)

Fig. 5. Examples of CLL histological images group.

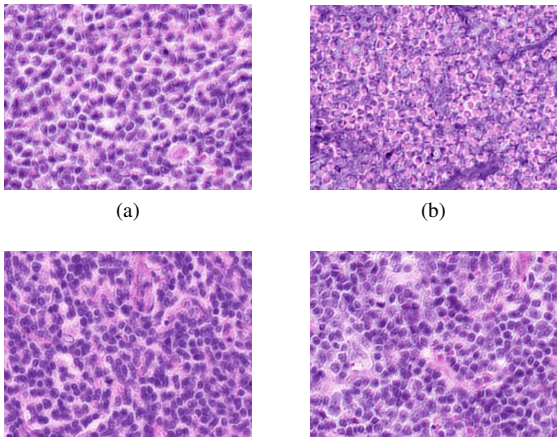

(a) (b) (c) (d)

Fig. 6. Examples of color normalized images (MCL group).

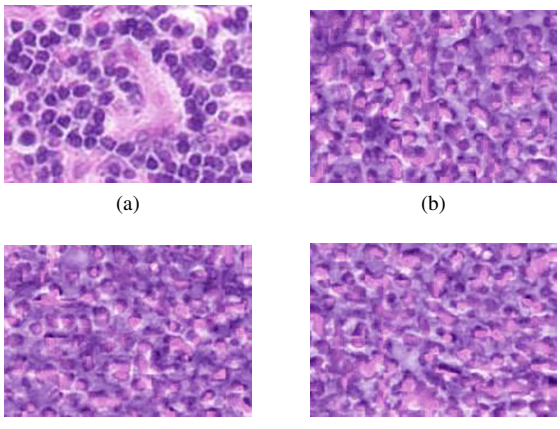

(a) (b) (c) (d)

Fig. 7. Examples of color normalized images, FL group.

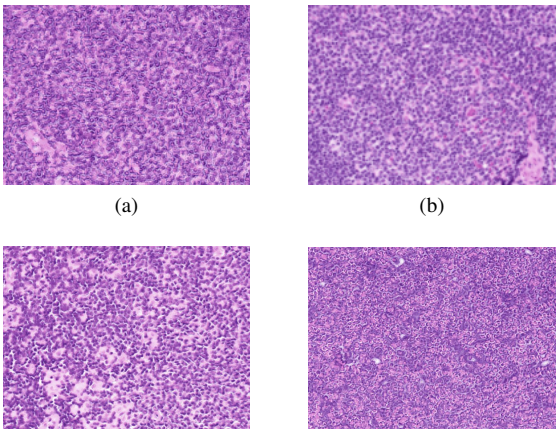

(a) (b) (c) (d)

Fig. 8. Examples of color normalized images (CLL group).

values from each image. The selection process was described in subsection II-F. The best observed case was achieved with 25 features per fold, with a number of 43 non-overlapping features. A list of the most selected features is presented on Table I.

TABLE I
ANALYSIS OF THE SELECTED FEATURES USING THE PROPOSED METHOD.

Approach	**Image type**	**Quantity**
FD_p	H&E Image	0
	Curvelet sub-image	0
FD_f	H&E Image	0
	Curvelet sub-image	0
Lac	H&E Image	1
	Curvelet sub-image	11
Har	H&E Image	3
	Curvelet sub-image	0
Perc	H&E Image	2
	Curvelet sub-image	26
	Total	43

From the results, it is possible to note that the features FD_p and FD_m were not selected, which may indicate that the fractal dimension and the combination with curvelet coefficients are not relevant for the differentiation of H&E lymphoma images. The selected Har features were extracted directly from the input images: variance, sum average and sum of variance. Finally the most selected features were multiscale and multidimensional lacunarity and percolation with 12 and 28 features, respectively. A number of 40 features (92.5%) was calculated from curvelet sub-images, indicating the importance of the association for distinguishing the group of interest.

An analysis was made considering the features that appeared in every fold in the selection step (Table II), wherein the percolation function $\Gamma(L)$ was the most selected, quantifying the average coverage ratio of the largest cluster. From $\Gamma(L)$, the maximum point (MP) was the most used feature. Most of the features were extracted from curvelet sub-images with scales 1 and 4. The curvelet sub-image with the highest number of extracted features was constituted of a combination of scale 1 and rotation 1.

TABLE II
MOST SELECTED FEATURES WITH CURVES METRICS FOR LAC AND PERC: ARC, SKW, AR, MP) AND SMP.

Feature	Image type
AR($Lac(L)$)	H&E
SKW($Lac(L)$)	Curvelet: Scale 1, Rotation 1
ARC($C(L)$) (Perc)	H&E
ARC($Q(L)$) (Perc)	Curvelet: Scale 1, Rotation 1
SMP($Q(L)$) (Perc)	Curvelet: Scale 1, Rotation 1
ARC($\Gamma(L)$) (Perc)	Curvelet: Scale 1, Rotation 1
AR($\Gamma(L)$) (Perc)	Curvelet: Scale 1, Rotation 1
MP($\Gamma(L)$) (Perc)	Curvelet: Scale 1, Rotation 1
SMP($\Gamma(L)$) (Perc)	Curvelet: Scale 1, Rotation 1
MP($\Gamma(L)$) (Perc)	Curvelet: Scale 4, Rotation 6
MP($\Gamma(L)$) (Perc)	Curvelet: Scale 4, Rotation 7
AR($\Gamma(L)$) (Perc)	Curvelet: Scale 4, Rotation 14
MP($\Gamma(L)$) (Perc)	Curvelet: Scale 4, Rotation 14
AR($\Gamma(L)$) (Perc)	Curvelet: Scale 4, Rotation 15
MP($\Gamma(L)$) (Perc)	Curvelet: Scale 4, Rotation 15

The selected features were applied to perform the classification. The results obtained in the classification considering the non-normalized images and normalized images comparing all three groups (MCLxFLxCLL) are presented on Table III. By the features extracted from the non-normalized images, it is noted that most of the classification techniques provided relevant results, with average AUC rates higher than 0.85. The highlight though is the classification with RaF approach achieving $AUC = 0.963$. When considering the normalized images, the results achieved were not relevant, where only the RaF classifier provided an AUC rate of 0.868.

Taking into consideration the AC measure, the results also are relevant for the non-normalized images, with the best cases comprising DT (86.14%) and RaF (85.03%). The obtained results were poor for the normalized cases. Another observation is that from the AC measure, the rates are slightly smaller when comparing with AUC. This fact is due to the unbalanced lymphoma classes compared, affecting the AC measure in the differentiation.

From such highlights, one can conclude that the best combination was achieved with the fractal attributes of lacunarity and percolation multiscale and multidimensional, both calculated from curvelet images and RaF classifier. Another observation was the lack of relevant differentiation rates when classifying the features extracted from color normalized images. A possible explanation is that the most relevant features were extracted from the curvelet sub-images instead of the extraction directly from the considered the images.

A variety of studies were developed for the lymphoma cancer detection, such as the works presented in [1], [5]–[7], [47], [48]. A comparison is presented in Table IV, based on the AC and AUC values observed from the cited methods.

The approaches proposed in Table IV presented AC higher than 85% by applying different methodologies. Each author proposed distinct methodologies which were relevant contributions in the literature. Although the direct comparison is a hard and unfair task, once each approach applied distinct methodologies and images datasets. Nevertheless, we believe

TABLE III
PERFORMANCE (AUC) FOR THE CLASSIFICATION OF THE GROUPS MCLXFLXCLL WITH THE PROPOSED COMBINATION OF FEATURES.

	Non-Normalized		Normalized	
Classifier	**AUC**	**AC**	**AUC**	**AC**
DT	0.873	86.14	0.705	64.05
SVM	0.837	82.12	0.649	61.76
RaF	0.963	85.03	0.868	73.39
NB	0.766	49.76	0.559	39.74
K*	0.852	71.16	0.699	64.12
Average	0.858	74.84	0.696	60.61

TABLE IV
PERFORMANCE OF THE PROPOSED METHOD AND CORRELATED WORKS BY CONSIDERAING AC AND AUC

Reference	**Features**	**Color**	**AC (%)**	**AUC**
Shamir et al. (2008) [47]	1,025	Yes	85.00	-
Meng et al. (2010) [48]	12,625	Yes	92.70	-
Orlov et al. (2010) [1]	1,025	Yes	99.00	-
Song et al. (2016) [5]	9,872	No	96.80	-
Codella et al. (2016) [6]	216	Yes	95.50	-
Roberto et al. (2017) [7]	15	Yes	96.40	0.967
Proposed method	43	Yes	86.14	0.963

that the proposed method is able to provide relevant results in the context of lymphoma images and the proposed method is compatible with the approaches observed in the specialized literature.

IV. CONCLUSION

In this work, a method was developed to extract features from non-normalized and color normalized lymphoma images, with a combination of multiscale and multidimensional fractal approaches, discrete curvelet transform and Haralick features. The classes distinguished were mantle cell lymphoma, follicular lymphoma and chronic lymphocytic leukemia.

The best case in the differentiation of the three groups was observed with multiscale and multidimensional percolation features extracted from curvelet sub-images (scales of 1 and 4), as well as quantifications performed with multiscale and multidimensional lacunarity, obtained from the non-normalized images and their curvelet sub-images calculated with scale 1.

The best classification rate was obtained with RaF classifier extracted from the images without color normalization. When considering the case of color normalized images, the results provided poor differentiation rates. We believe that this observation is due to the fact that most of the selected features were from curvelet sub-images, which were generated in gray levels, instead of the input images.

A comparison was performed with the correlated works. The proposed approach provided rates compatible with those observed in the literature. Moreover, we believe that the obtained results are relevant to the study of lymphomas, mainly in the comparison of non-normalized and color normalized images, allowing the analysis with different types of features and classifiers to differentiate 3 classes (MCL, FL, CLL). In future works, the authors expect to test the method in different color models, other curvelet scales and rotations, as well as apply different types of color normalization techniques for further investigations.

ACKNOWLEDGMENT

The authors thank to CNPq (427114/20160), CAPES (1646248) and FAPEMIG (TEC - APQ-02885-15) for financial support.

REFERENCES

[1] N. V. Orlov, W. W. Chen, D. M. Eckley, T. J. Macura, L. Shamir, E. S. Jaffe, and I. G. Goldberg, "Automatic classification of lymphoma images with transform-based global features," *IEEE Transactions on Information Technology in Biomedicine*, vol. 14, no. 4, pp. 1003–1013, 2010.

[2] R. L. Siegel, K. D. Miller, and A. Jemal, "Cancer statistics, 2018," *CA: a cancer journal for clinicians*, vol. 68, no. 1, pp. 7–30, 2018.

[3] INCA, "Estimate/2018 cancer incidence in brazil," Instituto Nacional de Câncer José Alencar Gomes da Silva, Rio de Janeiro, Brazil, Technical Report P-34, 2017.

[4] L. Xerri, S. Dirnhofer, L. Quintanilla-Martinez, B. Sander, J. K. Chan, E. Campo, S. H. Swerdlow, and G. Ott, "The heterogeneity of follicular lymphomas: from early development to transformation," *Virchows Archiv*, vol. 468, no. 2, pp. 127–139, 2016.

[5] Y. Song, W. Cai, H. Huang, D. Feng, Y. Wang, and M. Chen, "Bioimage classification with subcategory discriminant transform of high dimensional visual descriptors," *BMC bioinformatics*, vol. 17, no. 1, p. 465, 2016.

[6] N. Codella, M. Moradi, M. Matasar, T. Sveda-Mahmood, and J. R. Smith, "Lymphoma diagnosis in histopathology using a multi-stage visual learning approach," in *Medical Imaging 2016: Digital Pathology*, vol. 9791. International Society for Optics and Photonics, 2016, p. 97910H.

[7] G. F. Roberto, L. A. Neves, M. Z. Nascimento, T. A. Tosta, L. C. Longo, A. S. Martins, and P. R. Faria, "Features based on the percolation theory for quantification of non-hodgkin lymphomas," *Computers in Biology and Medicine*, vol. 91, pp. 135–147, 2017.

[8] R. M. Haralick, K. Shanmugam *et al.*, "Textural features for image classification," *IEEE Transactions on systems, man, and cybernetics*, vol. 3, no. 6, pp. 610–621, 1973.

[9] L. Boubchir, S. Al-Maadeed, and A. Bouridane, "Haralick feature extraction from time-frequency images for epileptic seizure detection and classification of eeg data," in *Microelectronics (ICM), 2014 26th International Conference on*. IEEE, 2014, pp. 32–35.

[10] S. Samanta, S. S. Ahmed, M. A.-M. M. Salem, S. S. Nath, N. Dey, and S. S. Chowdhury, "Haralick features based automated glaucoma classification using back propagation neural network," in *Proceedings of the 3rd International Conference on Frontiers of Intelligent Computing: Theory and Applications (FICTA) 2014*. Springer, 2015, pp. 351–358.

[11] M. Chakraborty, S. Mukhopadhyay, A. Dasgupta, S. Patsa, N. Anjum, and J. Ray, "A new approach of oral cancer detection using bilateral texture features in digital infrared thermal images," in *Engineering in Medicine and Biology Society (EMBC), 2016 IEEE 38th Annual International Conference of the*. IEEE, 2016, pp. 1377–1380.

[12] M. Ivanovici and N. Richard, "Fractal dimension of color fractal images," *IEEE Transactions on Image Processing*, vol. 20, no. 1, pp. 227–235, 2011.

[13] H. Gould, J. Tobochnik, D. C. Meredith, S. E. Koonin, S. R. McKay, and W. Christian, "An introduction to computer simulation methods: applications to physical systems," *Computers in Physics*, vol. 10, no. 4, pp. 349–349, 1996.

[14] D. Lamani, T. Manjunath *et al.*, "Fractal dimension with object rotation: a case study with glaucoma eye," in *Signal and Image Processing (ICSIP), 2014 Fifth International Conference on*. IEEE, 2014, pp. 111–116.

[15] T. Prabhakar and S. Poonguzhali, "Automatic detection and classification of benign and malignant lesions in breast ultrasound images using texture morphological and fractal features," in *Biomedical Engineering International Conference (BMEiCON), 2017 10th*. IEEE, 2017, pp. 1–5.

[16] L. A. Neves, M. Nascimento, D. Oliveira, A. S. Martins, M. Godoy, P. Arruda, D. de Santi Neto, and J. M. Machado, "Multi-scale lacunarity as an alternative to quantify and diagnose the behavior of prostate cancer," *Expert Systems with Applications*, vol. 41, no. 11, pp. 5017–5029, 2014.

[17] W.-C. Lin, C.-C. Li, C. S. Christudass, J. I. Epstein, and R. W. Veltri, "Curvelet-based classification of prostate cancer histological images of critical gleason scores," in *Biomedical Imaging (ISBI), 2015 IEEE 12th International Symposium on*. IEEE, 2015, pp. 1020–1023.

[18] D. Saraswathi, D. Dharani, and E. Srinivasan, "An efficient feature extraction technique for breast cancer diagnosis using curvelet transform and swarm intelligence," in *Wireless Communications, Signal Processing and Networking (WiSPNET), International Conference on*. IEEE, 2016, pp. 441–445.

[19] D. R. Nayak, R. Dash, B. Majhi, and V. Prasad, "Automated pathological brain detection system: A fast discrete curvelet transform and probabilistic neural network based approach," *Expert Systems with Applications*, vol. 88, pp. 152–164, 2017.

[20] T. Schäfer, H. Schäfer, A. Schmitz, J. Ackermann, N. Dichter, C. Döring, S. Hartmann, M.-L. Hansmann, and I. Koch, "Image database analysis of hodgkin lymphoma," *Computational biology and chemistry*, vol. 46, pp. 1–7, 2013.

[21] A. Vahadane, T. Peng, A. Sethi, S. Albarqouni, L. Wang, M. Baust, K. Steiger, A. M. Schlitter, I. Esposito, and N. Navab, "Structure-preserving color normalization and sparse stain separation for histological images," *IEEE transactions on medical imaging*, vol. 35, no. 8, pp. 1962–1971, 2016.

[22] M. N. Gurcan, L. E. Boucheron, A. Can, A. Madabhushi, N. M. Rajpoot, and B. Yener, "Histopathological image analysis: A review," *IEEE reviews in biomedical engineering*, vol. 2, pp. 147–171, 2009.

[23] J. A. A. Jothi and V. M. A. Rajam, "A survey on automated cancer diagnosis from histopathology images," *Artificial Intelligence Review*, vol. 48, no. 1, pp. 31–81, 2017.

[24] M. Macenko, M. Niethammer, J. Marron, D. Borland, J. T. Woosley, X. Guan, C. Schmitt, and N. E. Thomas, "A method for normalizing histology slides for quantitative analysis," in *Biomedical Imaging: From Nano to Macro, 2009. ISBI'09. IEEE International Symposium on*. IEEE, 2009, pp. 1107–1110.

[25] D. Magee, D. Treanor, D. Crellin, M. Shires, K. Smith, K. Mohee, and P. Quirke, "Colour normalisation in digital histopathology images," in *Proc. optical tissue image analysis in microscopy, histopathology and endoscopy (MICCAI workshop)*. Citeseer, 2009, pp. 100–111.

[26] E. Candes, L. Demanet, D. Donoho, and L. Ying, "Fast discrete curvelet transforms," *Multiscale Modeling & Simulation*, vol. 5, no. 3, pp. 861–899, 2006.

[27] G. Liu, G. Yan, S. Kuang, and Y. Wang, "Detection of small bowel tumor based on multi-scale curvelet analysis and fractal technology in capsule endoscopy," *Computers in biology and medicine*, vol. 70, pp. 131–138, 2016.

[28] V. S. Charisis and L. J. Hadjileontiadis, "Potential of hybrid adaptive filtering in inflammatory lesion detection from capsule endoscopy images," *World Journal of Gastroenterology*, vol. 22, no. 39, p. 8641, 2016.

[29] M. Ivanovici, N. Richard, and H. Decean, "Fractal dimension and lacunarity of psoriatic lesions-a colour approach," *medicine*, vol. 6, no. 4, p. 7, 2009.

[30] N. Nikolaidis, I. Nikolaidis, and C. Tsouros, "A variation of the box-counting algorithm applied to colour images," *arXiv preprint arXiv:1107.2336*, 2011.

[31] N. Bird and E. Perrier, "Multiscale percolation properties of a fractal pore network," *Geoderma*, vol. 160, no. 1, pp. 105–110, 2010.

[32] J. Hoshen and R. Kopelman, "Percolation and cluster distribution. i. cluster multiple labeling technique and critical concentration algorithm," *Physical Review B*, vol. 14, no. 8, p. 3438, 1976.

[33] R. F. Voss, "Random fractals: characterization and measurement," in *Scaling phenomena in disordered systems*. Springer, 1991, pp. 1–11.

[34] R. E. Plotnick, R. H. Gardner, W. W. Hargrove, K. Prestegaard, and M. Perlmutter, "Lacunarity analysis: a general technique for the analysis of spatial patterns," *Physical review E*, vol. 53, no. 5, p. 5461, 1996.

[35] I. Kononenko, E. Šimec, and M. Robnik-Šikonja, "Overcoming the myopia of inductive learning algorithms with relieff," *Applied Intelligence*, vol. 7, no. 1, pp. 39–55, 1997.

[36] M. Robnik-Šikonja and I. Kononenko, "Theoretical and empirical analysis of relieff and rrelieff," *Machine learning*, vol. 53, no. 1-2, pp. 23–69, 2003.

[37] M. B. Al Snousy, H. M. El-Deeb, K. Badran, and I. A. Al Khlil, "Suite of decision tree-based classification algorithms on cancer gene expression data," *Egyptian Informatics Journal*, vol. 12, no. 2, pp. 73–82, 2011.

[38] V. N. Vapnik, "An overview of statistical learning theory," *IEEE transactions on neural networks*, vol. 10, no. 5, pp. 988–999, 1999.

[39] L. Breiman, "Random forests," *Machine learning*, vol. 45, no. 1, pp. 5–32, 2001.

[40] S. B. Kotsiantis, I. Zaharakis, and P. Pintelas, "Supervised machine learning: A review of classification techniques," 2007.

[41] D. Y. Mahmood and M. A. Hussein, "Intrusion detection system based on k-star classifier and feature set reduction," *IOSR Journal of Computer Engineering*, vol. 15, no. 5, pp. 107–12, 2013.

[42] T. Fawcett, "Roc graphs: Notes and practical considerations for researchers," *Machine learning*, vol. 31, no. 1, pp. 1–38, 2004.

[43] I. H. Witten, E. Frank, M. A. Hall, and C. J. Pal, *Data Mining: Practical machine learning tools and techniques*. Morgan Kaufmann, 2016.

[44] L. Demanet, "The curvelet organization," http://www.curvelet.org/software.html, 2008, accessed: 05.26.2018.

[45] N. I. on Aging, https://www.nia.nih.gov/, accessed: 05.28.2018.

[46] N. C. Institute, https://www.cancer.gov/, accessed: 05.28.2018.

[47] L. Shamir, N. Orlov, D. M. Eckley, T. J. Macura, and I. G. Goldberg, "Iicbu 2008: a proposed benchmark suite for biological image analysis," *Medical & biological engineering & computing*, vol. 46, no. 9, pp. 943–947, 2008.

[48] T. Meng, L. Lin, M.-L. Shyu, and S.-C. Chen, "Histology image classification using supervised classification and multimodal fusion," in *Multimedia (ISM), 2010 IEEE International Symposium on*. IEEE, 2010, pp. 145–152.